Journal of the Brazilian Society of Mechanical Sciences and Engineering (2019) 41:4
https://doi.org/10.1007/s40430-018-1482-0

TECHNICAL PAPER

Consequences of activation energy and binary chemical reaction for 3D flow of Cross-nanofluid with radiative heat transfer

W. A. Khan[1] · F. Sultan[1,2] · M. Ali[1] · M. Shahzad[1] · M. Khan[3] · M. Irfan[3]

Received: 25 February 2018 / Accepted: 5 November 2018 / Published online: 27 November 2018

Abstract
In view of ecological concern and energy security, execution of refrigeration system should be enriched which can be done by improving the characteristics of working liquids. The nanoliquids have gained interest in industrial and engineering fields due to their outstanding thermophysical features. Researchers used nanoliquids as working liquid and detected substantial variations in thermal performance. In the present research work, our intention is to explore the impact of nonlinear thermal radiation and variable thermal conductivity on 3D flow of cross-nanofluid. Moreover, heat sink–source, chemical processes and activation energy are implemented. Zero mass flux relation with thermophoresis and Brownian motion mechanisms are scrutinized. The required system of ordinary ones is achieved by implementing appropriate transformations. The achieved system of ordinary ones is computed numerically by implementing bvp4c scheme. Graphs are plotted to explore the impact of various physical parameters on concentration, temperature and velocity fields. It is detected from obtained graphical data that thermophoresis and Brownian motion mechanisms significantly affect heat transport mechanism. Furthermore, graphical analysis reveals that concentration of cross-nanofluid enhances for augmented values of activation energy.

Keywords 3D flow · Activation energy · Cross-fluid model · Nanoparticles · Nonlinear thermal radiation · New mass flux boundary conditions

List of symbols

u, v, w	Velocity components (ms^{-1})
x, y, z	Space coordinates (ms^{-1})
n	Power law index
m	Fitted rate constant
$(\rho c)_f$	Heat capacity of fluid
T	Temperature of fluid (K)
$k(T)$	Variable thermal conductivity $\left(\frac{\mathrm{W}}{\mathrm{mK}}\right)$
α_1	Thermal diffusivity (ms^{-1})
k^*	Boltzmann constant
D_B	Brownian diffusion coefficient
D_T	Thermophoresis diffusion coefficient $\left(\frac{\mathrm{m}^2}{\mathrm{s}}\right)$
C	Nanoparticles concentration (K)
Q_0	Dimensional heat source/sink parameter
E_a	Activation energy
a, b	Positive constants
B_0	Magnetic field strength $\left(\frac{\mathrm{A}}{\mathrm{M}}\right)$
C_∞	Ambient concentration
T_∞	Ambient fluid temperature (K)
k_∞	Thermal conductivity far away from stretched surface
h_f	Heat conversion coefficient $\left(\frac{\mathrm{W}}{\mathrm{Km}^2}\right)$
f, g	Dimensionless velocities
C_{fx}, C_{fy}	Skin fractions
Nu_x	Local Nusselt number
M	Magnetic parameter
$U_w(x,t), V_w(y,t)$	Stretching velocities (ms^{-1})
E	Activation energy
We_1, We_2	Local Weissenberg numbers
Pr	Prandtl number
Le	Lewis number
q_r	Nonlinear radiative heat flux

Technical Editor: Cezar Negrao, PhD.

✉ W. A. Khan
waqar_qau85@yahoo.com

[1] Department of Mathematics, Hazara University, Mansehra, Pakistan

[2] Department of Mathematical Analysis, Ghent University, Ghent, Belgium

[3] Department of Mathematics, Quaid-i-Azam University, Islamabad 44000, Pakistan

N_b	Brownian motion parameter
N_t	Thermophoresis parameter
R_d	Radiation parameter
$(\rho c)_\mathrm{p}$	Effective heat capacity of a nanoparticle
Re_x	Local Reynolds number
α	Ratio of stretching rates parameter
k_c	Chemical reaction constant

Greek symbols

γ	Biot number
τ	Effective heat capacity ratio
λ	Dimensionless heat source or sink parameter
ϕ	Dimensionless concentration
σ	Stefan–Boltzmann constant $\left(\frac{\mathrm{S}}{\mathrm{m}}\right)$
η	Dimensionless variable
θ_f	Temperature ratio parameter
ρ_f	Fluid density $\left(\frac{\mathrm{kg}}{\mathrm{m}^3}\right)$
θ	Dimensionless temperature
ε	Thermal conductivity parameter
ν	Kinematics viscosity $\left(\mathrm{m}^2\mathrm{s}^{-1}\right)$

1 Introduction

Recent innovative methodologies have paved the way for the appearance of manufactured materials at nanometer scale. Nanoliquid possesses huge impact on the improvement of newly developed heat transfer liquids. Nanoliquid is innovative engineered materials having massive applications in biology, cancer diagnosis, nuclear industries, drilling and oil recovery. Moreover, nanofluids have been widely utilized for heat transport applications. Khan et al. [1] inspected the impact of heat sink–source and nanoparticles on an Oldroyd-B fluid. Sheikholeslami and Ellahi [2] considered the characteristics of cubic cavity for 3D flow of magneto-nanofluid. Khan and Khan [3] reported the analysis for Burgers fluid in existence of nanoparticles. Sandeep et al. [4] investigated the impact of convective heat/mass transfer mechanisms on non-Newtonian magneto-nanofluid. Rehman et al. [5] studied the characteristics of entropy generation by utilizing nanoparticles. Khan and Khan [6] demonstrated impact of zero mass flux condition for power-law nanofluid. Haq et al. [7] utilized two-phase relation for water and ethylene glycol-based Cu nanoparticles under effect of suction–injection. Steady-state 2D flow of Burgers fluid in existence of nanoparticles was demonstrated by Khan and Khan [8]. Zero mass flux relation has been employed by Khan et al. [9] to visualize behavior of Burgers fluid in the presence of nanoparticles. Rahman et al. [10] reported nanofluid flow for Jeffrey fluid. Raju et al. [11] studied the magneto-nanofluid flow in the presence of rotating cone with temperature-dependent viscosity. Recently, numerous investigators published their research work about heat transport [12–37].

Disparity of concentration in chemically reacting species effecting on mass transfer mechanism. In these situations, chemical species moves from high to low concentrated area. Applications of chemical reactions include manufacturing of food, formation and dispersion of fog, manufacturing of ceramics, production of polymer, crops damage via freezing, hydrometallurgical industry, geothermal reservoirs, cooling of nuclear reactor and recovery of thermal oil. Some reactions have capacity to move slowly or not at all except in the existence of a catalyst. Activation energy plays an important role in enhancing the production speed of chemical reactions. Moreover, activation energy is smallest amount of energy that reactants must acquire to start a chemical reaction. The term activation energy was initially presented by Arrhenius in 1889. The applications of activation energy are very wide in geothermal, mechanics of water, chemical engineering and oil emulsions. Khan et al. [38] considered the chemical processes for 3D flow of Burgers fluid by utilizing the revised heat–mass flux relations. Khan et al. [39] analyzed the effects of chemical processes on 3D flow of Burgers fluid. Khan et al. [40] investigated the characteristics of convective flow in the presence of variable thicked surface. Khan et al. [41] examined the features of revised heat flux relation and chemical processes for Maxwell fluid. Khan et al. [42] inspected the impact of chemical reactions on generalized Burgers fluid by utilizing the nanoparticles. Mustafa et al. [43] examined the characteristics of activation energy and chemical mechanisms on magneto-nanofluid.

Our main focus here is to explore the impact of activation energy on 3D flow of cross-nanofluid with combined effects of heat sink–source and nonlinear thermal radiation. Heat transport phenomenon is scrutinized through variable thermal conductivity. Moreover, impacts of chemical processes and Lorentz's forces are accounted. By employing transformations procedure, the governing PDE's are converted into ODE's which are then tackled numerically by bvp4c. Outcomes of physical parameters involved in this research work are analyzed through graphical and tabular data.

2 Physical model and problem statement

Geometry and boundary condition of physical model for steady 3D forced convective flow of cross-nanofluid is presented through Fig. 1. In this research work, we have utilized the thermally heated surface which can be utilized for various industrial products. Coordinate system is selected in such a way that sheet coincides with the plane $z = 0$ and motion of the cross-nanofluid is confined in the half space $z > 0$. Aspects of heat sink–source and thermal radiation are carried out in existing flow situation. Mass transport

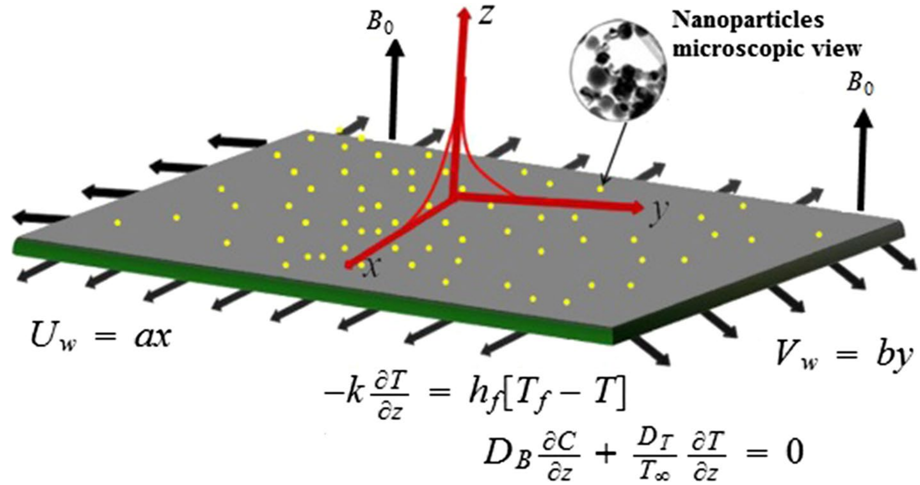

Fig. 1 Physical geometry for the problem

mechanism is scrutinized through activation energy. We have applied magnetic field of strength B_0 in z-direction. Furthermore, the impact of induced magnetic field on the cross-nanofluid is neglected by utilizing the assumption of low Reynolds number. The sheet is kept at constant concentration C_w, whereas the nanofluid outside the boundary is maintained at uniform temperature and concentration (T_∞, C_∞), respectively. In areas such as geothermal, the governing equations are [see Ref. 9, 44]:

$$\frac{\partial u}{\partial x} + \frac{\partial v}{\partial y} + \frac{\partial w}{\partial z} = 0, \tag{1}$$

$$u\frac{\partial u}{\partial x} + v\frac{\partial u}{\partial y} + w\frac{\partial u}{\partial z} = -\frac{1}{\rho_f}\frac{\partial P}{\partial x} + \nu\frac{\partial}{\partial z}\left[\frac{\frac{\partial u}{\partial z}}{1+\left\{\Gamma\left(\frac{\partial u}{\partial z}\right)\right\}^n}\right] - \frac{\sigma_1 B_0^2 u}{\rho_f}, \tag{2}$$

$$u\frac{\partial v}{\partial x} + v\frac{\partial v}{\partial y} + w\frac{\partial v}{\partial z} = -\frac{1}{\rho_f}\frac{\partial P}{\partial y} + \nu\frac{\partial}{\partial z}\left[\frac{\frac{\partial v}{\partial z}}{1+\left\{\Gamma\left(\frac{\partial v}{\partial z}\right)\right\}^n}\right] - \frac{\sigma_1 B_0^2 v}{\rho_f}, \tag{3}$$

$$\begin{aligned} u\frac{\partial T}{\partial x} + v\frac{\partial T}{\partial y} + w\frac{\partial T}{\partial z} &= \frac{1}{(\rho c)_f}\frac{\partial}{\partial z}\left(k(T)\frac{\partial T}{\partial z}\right) \\ &+ \tau\left[D_B\frac{\partial C}{\partial z}\frac{\partial T}{\partial z} + \frac{D_T}{T_\infty}\left(\frac{\partial T}{\partial z}\right)^2\right] \\ &- \frac{1}{(\rho c)_f}\frac{\partial q_r}{\partial z} + \frac{Q_0}{(\rho c)_f}(T - T_\infty), \end{aligned} \tag{4}$$

$$\begin{aligned} u\frac{\partial C}{\partial x} + v\frac{\partial C}{\partial y} + w\frac{\partial C}{\partial z} &= D_B\frac{\partial^2 C}{\partial z^2} + \frac{D_T}{T_\infty}\frac{\partial^2 T}{\partial z^2} \\ &- k_c^2(C - C_\infty)\left(\frac{T}{T_\infty}\right)^m \exp\left(-\frac{E_a}{k^* T}\right). \end{aligned} \tag{5}$$

with

$$\begin{aligned} &u = U_w = ax, \quad v = V_w = by, \quad w = 0, \\ &-k\frac{\partial T}{\partial z} = h_f[T_f - T],\ D_B\frac{\partial C}{\partial z} + \frac{D_T}{T_\infty}\frac{\partial T}{\partial z} = 0 \quad \text{at} \quad z = 0, \end{aligned} \tag{6}$$

$$u \to 0,\ v \to 0,\ T \to T_\infty,\ C \to C_\infty \quad \text{as} \quad z \to \infty, \tag{7}$$

where

$$k(T) = k_\infty\left(1 + \varepsilon\left(\frac{T - T_\infty}{T_f - T_\infty}\right)\right), \tag{8}$$

$$q_r = -\frac{4\sigma^*}{3k^*}\frac{\partial T^4}{\partial z} = -\frac{16\sigma^*}{3k^*}\frac{\partial}{\partial z}\left(T^3\frac{\partial T}{\partial z}\right), \tag{9}$$

Substituting Eqs. (8) and (9) into Eq. (4), we have the following energy equation

$$\begin{aligned} u\frac{\partial T}{\partial x} + v\frac{\partial T}{\partial y} + w\frac{\partial T}{\partial z} &= \frac{1}{(\rho c)_f}\frac{\partial}{\partial z}\left(k(T)\frac{\partial T}{\partial z}\right) \\ &+ \tau\left[D_B\frac{\partial C}{\partial z}\frac{\partial T}{\partial z} + \frac{D_T}{T_\infty}\left(\frac{\partial T}{\partial z}\right)^2\right] \\ &+ \frac{1}{(\rho c)_f}\frac{16\sigma^*}{3k^*}\frac{\partial}{\partial z}\left(T^3\frac{\partial T}{\partial z}\right) + \frac{Q_0}{(\rho c)_f}(T - T_\infty). \end{aligned} \tag{10}$$

Considering the following suitable conversions,

$$u = axf'(\eta), \quad v = ayg'(\eta), \quad w = -(a\nu)^{\frac{1}{2}}\left[f(\eta) + g(\eta)\right],$$
$$\theta(\eta) = \frac{T - T_\infty}{T_f - T_\infty}, \quad \varphi(\eta) = \frac{C - C_\infty}{C_\infty}, \quad \eta = z\sqrt{\frac{a}{\nu}}. \tag{11}$$

Equation (1) is automatically satisfied, and Eqs. (2)–(7) and (9) yield

$$\left[1 + (1-n)\left(We_1 f''\right)^n\right] f''' - \left[1 + \left(We_1 f''\right)^n\right]^2 \left[f'^2 - (f+g)f'' + M^2 f'\right] = 0, \tag{12}$$

$$\left[1 + (1-n)\left(We_2 g''\right)^n\right] g''' - \left[1 + \left(We_2 g''\right)^n\right]^2 \left[g'^2 - (f+g)g'' + M^2 g'\right] = 0, \tag{13}$$

$$\frac{d}{d\eta}\left[\{1 + R_d\{1 + (\theta_f - 1)\theta\}^3\}\theta'\right] + (\varepsilon\theta)\theta'' + \varepsilon\theta'^2 + Pr\left[(f+g)\theta' + N_b\theta'\varphi' + N_t\theta'^2\right] + Pr\,\lambda\theta = 0, \tag{14}$$

$$\varphi'' + Le\,Pr(f+g)\varphi' - Le\,Pr\,\sigma\varphi(1+\delta\theta)^m \exp\left(-\frac{E}{1+\delta\theta}\right) + \frac{N_t}{N_b}\theta'' = 0, \tag{15}$$

$$f = 0, \quad g = 0, \quad f' = 1, \quad g' = \alpha,$$
$$\theta'(0) = -\gamma[1 - \theta(0)], \quad N_b\varphi'(0) + N_t\theta'(0) = 0, \quad \text{at} \quad \eta = 0, \tag{16}$$

$$f' \to 0, \quad g' \to 0, \quad \theta \to 0, \quad \varphi \to 0, \quad \text{as} \quad \eta \to \infty. \tag{17}$$

Mathematically, dimensionless parameters are defined as

$$We_1 = \Gamma ax\sqrt{\frac{a}{\nu}},\ We_2 = \Gamma ay\sqrt{\frac{a}{\nu}},\ R_d = \frac{16\sigma^* T_\infty^3}{3k_\infty k^*},\ \alpha = \frac{b}{a},\ \theta_f = \frac{T_f}{T_\infty},$$
$$M = \frac{\sigma_1 B_0^2}{\rho_f a},\ N_b = \frac{\tau D_B C_\infty}{\nu},\ N_t = \frac{\tau D_T(T_f - T_\infty)}{\nu T_\infty},\ \lambda = \frac{Q_0}{a(\rho c)_f},$$
$$Pr = \left(\frac{\nu}{\alpha_1}\right),\ Le = \frac{\alpha_1}{D_B},\ \sigma = \frac{k_c^2}{a},\ E = \frac{E_a}{k^* T_\infty},\ \delta = \frac{T_f - T_\infty}{T_\infty}, \tag{18}$$

The mathematical relations of local skin frictions, local Nusselt number and local Sherwood number in dimensional form are expressed as

$$C_{f_x} = \frac{2\tau_{xz}}{\rho_f U_w^2}, \quad C_{f_y} = \frac{2\tau_{yz}}{\rho_f U_w^2}, \tag{19}$$

$$Nu_x = -\frac{x}{\left(T_f - T_\infty\right)}\left(\frac{\partial T}{\partial z}\right)\bigg|_{z=0} + \frac{xq_r}{k\left(T_f - T_\infty\right)}, \tag{20}$$

$$Sh_x = -\frac{x}{\left(C_f - C_\infty\right)}\left(\frac{\partial C}{\partial z}\right)\bigg|_{z=0}. \tag{21}$$

Dimensionless form of overhead physical quantities is

$$C_{f_x}\left(Re_x\right)^{\frac{1}{2}} = \frac{2f''(0)}{\left[1 + \left(We_1 f''(0)\right)^n\right]},$$
$$C_{f_y}\left(Re_y\right)^{-\frac{1}{2}} = \frac{2V_w g''(0)}{U_w\left[1 + \left(We_2 g''(0)\right)^n\right]}, \tag{22}$$

$$\left(Re_x\right)^{-\frac{1}{2}} Nu_x = -\left[1 + R_d\{1 + (\theta_f - 1)\theta\}^3\right]\theta'(0), \tag{23}$$

where

$$Re_x = \frac{ax^2}{\nu}.$$

3 Numerical procedure

In this research work, bvp4c method is implemented for the considered problem. In this regard, system of ODEs along with boundary conditions is converted into system of first-order differential equations and solved numerically for involved physical parameters.

$$f = s_1, \quad f' = s_2, \quad f'' = s_3, \quad f''' = s_3', \tag{24}$$

$$g = s_4, \quad g' = s_5, \quad g'' = s_6, \quad g''' = s_6', \tag{25}$$

$$\theta = s_7, \quad \theta' = s_8, \quad \theta'' = s_8', \tag{26}$$

$$\varphi = s_9, \quad \varphi' = s_{10}, \quad \varphi'' = s_{10}', \tag{27}$$

where

$$s_3' = \frac{\left(1 + (We_1 s_3)^n\right)^2 (M^2 s_2 + s_2^2 - (s_1 + s_4)s_3)}{A_1}, \tag{28}$$

here

$$s_6' = \frac{\left(1 + (We_2 s_6)^n\right)^2 (M^2 s_5 + s_5^2 - (s_1 + s_4)s_6)}{A_2}, \tag{29}$$

$$A_1 = 1 + (1-n)\left(We_1 s_3\right)^n, \tag{30}$$

$$A_2 = 1 + (1-n)\left(We_2 s_6\right)^n, \tag{31}$$

$$s_8' = \frac{-Pr((s_1+s_4)s_8 + N_b s_8 s_{10} + N_t s_8^2 - \lambda s_7)}{A_3} \frac{-\varepsilon s_8^2 - 3R_d(1+(\theta_f-1)s_7)^2(\theta_f-1)s_8^2}{A_3}, \tag{32}$$

here

$$A_3 = 1 + \varepsilon s_7 + R_d\left(1 + \left(\theta_f - 1\right) s_7\right)^3, \tag{33}$$

$$s_{10}' = -Pr\,Le(s_1+s_4)s_{10} + Pr\,Le\sigma((1+\delta s_7)^m) \times \exp(-E/(1+\delta s_7))s_9 - \frac{N_t}{N_b} s_8', \tag{34}$$

with

$$s_1(0)=0,\ s_4(0)=0,\ s_2(0)=1,\ s_5(0)=\alpha,\ s_8(0)+\gamma\left(1-s_7(0)\right)=0,\ N_b s_{10}(0)+N_t s_8(0)=0, \tag{35}$$

$$s_2 \to 0, \quad s_5 \to 0, \quad s_7 \to 0, \quad s_9 \to 0 \quad \text{as} \quad \eta \to \infty. \tag{36}$$

3.1 Validation with previous results

Table 1 certifies the appropriateness of obtained numerical outcomes by making a comparison for Newtonian fluid with the outcomes tabulated by Ariel [44]. The numerical data for $-f''(0)$ and $-g''(0)$ are computed, and legitimacy of work is ensured.

4 Physical analysis

In the current research work, impact of activation energy and Lorentz forces on 3D forced convective flow of cross-nanofluid is demonstrated. Zero mass flux relation is employed for estimating cross-nanofluid properties. Features of heat transport for nanofluid are scrutinized through nonlinear radiation and heat source–sink. Numerical data of the present investigation are declared in terms of profiles of velocity, temperature and concentration. The surface drag forces, heat transfer rate and mass transfer rate for fluctuating various parameters are illustrated through tables.

4.1 Velocity profile

Figure 2a, b is plotted to demonstrate the behavior of velocity profile corresponding to change in local Weissenberg number We. It is observed from graphical that velocity of cross-nanofluid declines for augmented values of We_1 and We_2. Physical reason behind this behavior of cross-nanofluid is that as we raise value of We_1 and We_2 relaxation time enhances due to which velocity of cross-nanofluid deteriorates. Figure 3a, b presents the impact of n on velocity of cross-nanofluid. The examination of these figures reveals that progressive trend of velocity profile rises for shear-thinning regime. Physically, an uplift in the value of n less resistance is faced by shear-thinning fluid due to low viscosity which causes an enlargement in fluid velocity.

4.2 Temperature field

Figures 4, 5, 6, 7 and 8 are portrayed here to investigate the impact of α, N_t, λ, θ_f and γ for $n < 1$ and $n > 1$ on temperature of cross-nanofluid. To exhibit the effects of α on

Table 1 A comparison of $f''(0)$ and $g''(0)$ for Newtonian fluid with $We_1 = We_2 = M = 0$

β	Exact result [44] $-f''(0)$	Exact result [44] $-g''(0)$	HPM result [44] $f''(0)$	HPM result [44] $g''(0)$	Present result $f''(0)$	Present result $-g''(0)$
0.0	1.0	0.0	1.0	0.0	1.0	0.0
0.1	1.020259	0.066847	1.02025	0.06684	1.02026	0.06685
0.2	1.039495	0.148736	1.03949	0.14873	1.03949	0.14874
0.3	1.05794	0.243359	1.05795	0.24335	1.05795	0.24336
0.4	1.075788	0.349208	1.07578	0.34920	1.07578	0.34921
0.5	1.093095	0.465204	1.09309	0.46520	1.09309	0.46521
0.6	1.109946	0.590528	1.10994	0.59052	1.10994	0.59053
0.7	1.126397	0.724531	1.12639	0.72453	1.12639	0.72453
08	1.142488	0.866682	1.14248	0.86668	1.14249	0.86668
0.9	1.158253	1.01653	1.15825	1.01653	1.15826	1.016538
1.0	1.173720	1.173720	1.17372	1.17372	1.17372	1.17372

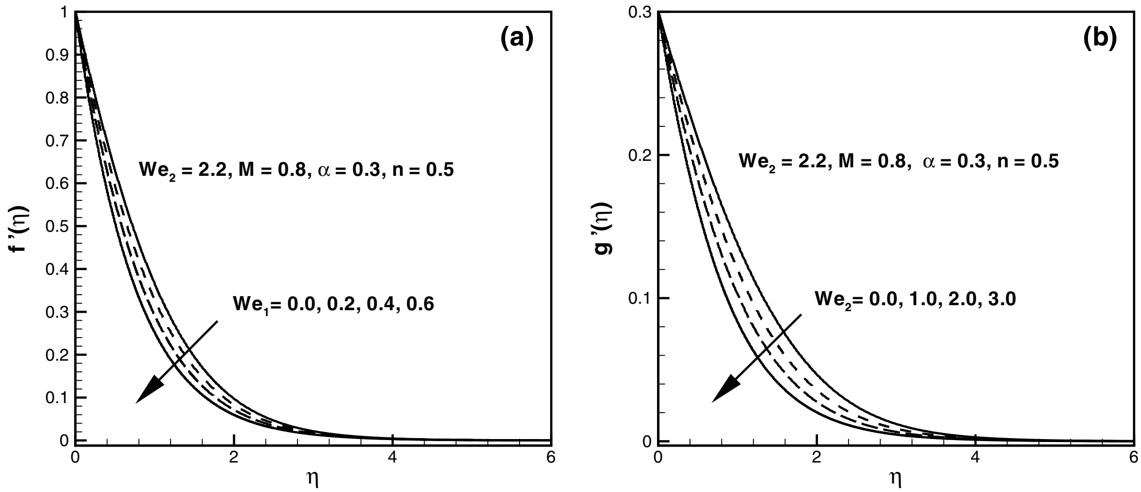

Fig. 2 Profiles of velocity $f'(\eta)$ for various values of We_1 for shear-thinning (**a**) and profiles of velocity $g'(\eta)$ for various values of We_2 for shear-thinning (**b**)

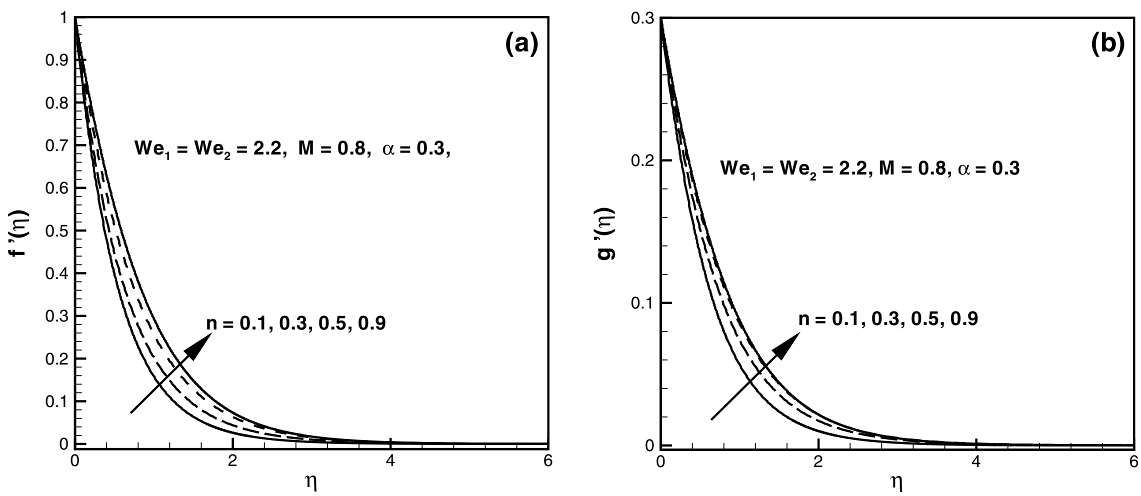

Fig. 3 Profiles of velocity $f'(\eta)$ for various values of n for shear-thinning (**a**) and profiles of velocity $g'(\eta)$ for various values of n for shear-thinning (**b**)

the temperature profile of cross-nanofluid, we have plotted Fig. 4a, b. These sketches show that the temperature of cross-nanofluid decreases as the values of α are augmented. Furthermore, careful analysis of these sketches releases that decaying behavior of cross-nanofluid is more prominent for $n < 1$. Figure 5a, b interprets the dependence of thermophoresis parameter N_t on the temperature of cross-nanofluid. The rise in the temperature of cross-nanofluid is detected for growing values of N_t. Physically, N_t demonstrates the temperature difference of cross-nanofluid between the hot fluid behind the sheet and temperature of liquid at infinity. The ratio of hot fluid behind the sheet to temperature of liquid at infinity θ_f and heat absorption parameter λ play a vital role in forced convective 3D flow of cross-nanofluid. Figures 6a, b and 7a, b present the impact of λ and θ_f on temperature profile of cross-nanofluid. These figures depict that the augmented values of θ_f and λ affect the heat transfer strongly. Physically, as θ_f strengthens, the temperature of the wall become higher as compared to temperature of the nanoliquid at infinity. Thus, as a result, the temperature of nanofluid enhances. Figure 8a, b is sketched to perceive the dependence of 3D flow of cross-nanofluid on γ for $n < 1$ and $n > 1$. The exploration of these plots impart that Biot number leads to enhancement of nanofluid temperature. Physical reason behind this trend of γ is that less resistance is faced by the thermal wall which causes an enhancement in convective heat transfer to the fluid.

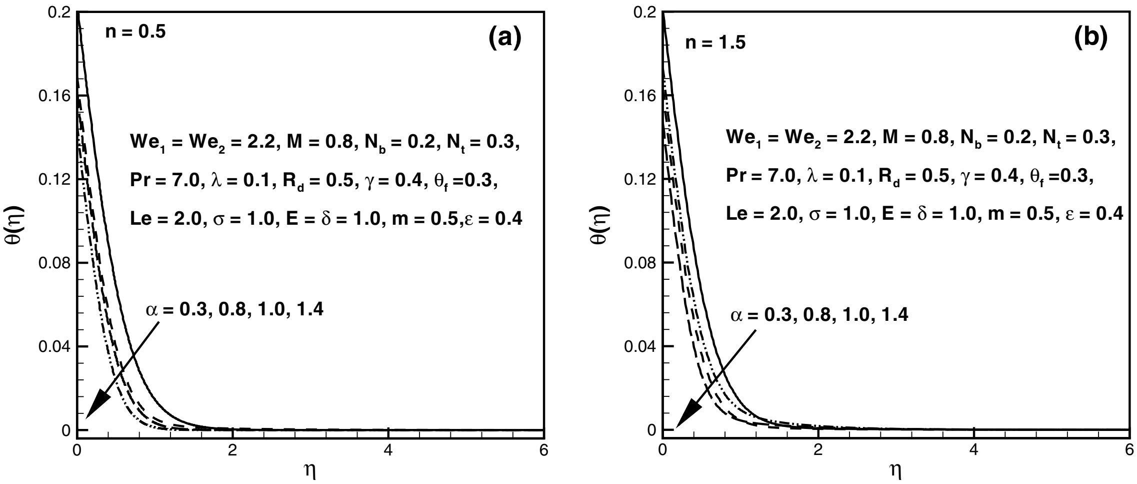

Fig. 4 Profiles of temperature $\theta(\eta)$ for various values of α for shear-thinning (**a**) and shear-thickening liquids (**b**)

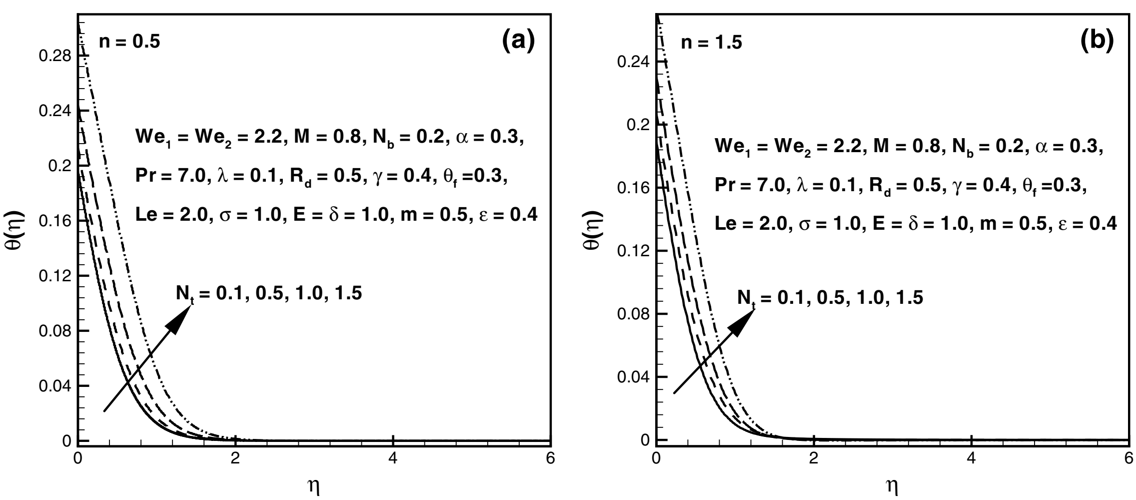

Fig. 5 Profiles of temperature $\theta(\eta)$ for various values of N_t for shear-thinning (**a**) and shear-thickening liquids (**b**)

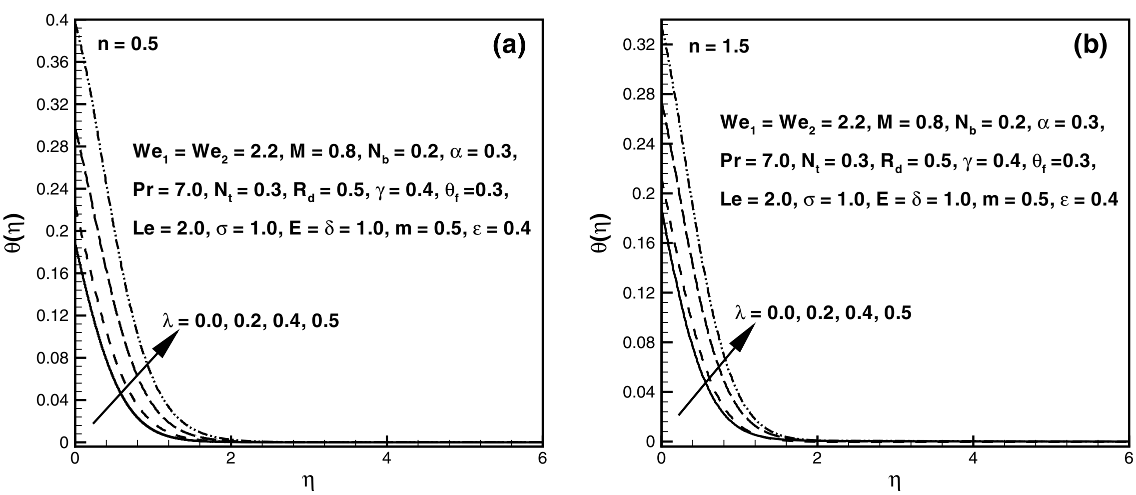

Fig. 6 Profiles of temperature $\theta(\eta)$ for various values of λ for shear-thinning (**a**) and shear-thickening liquids (**b**)

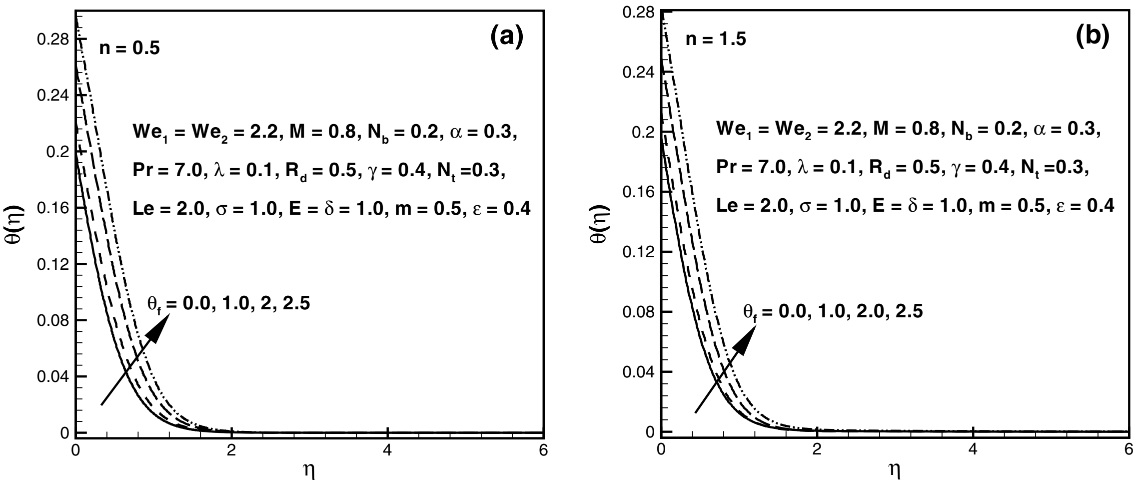

Fig. 7 Profiles of concentration $\varphi(\eta)$ for various values of θ_f for shear-thinning (**a**) and shear-thickening liquids (**b**)

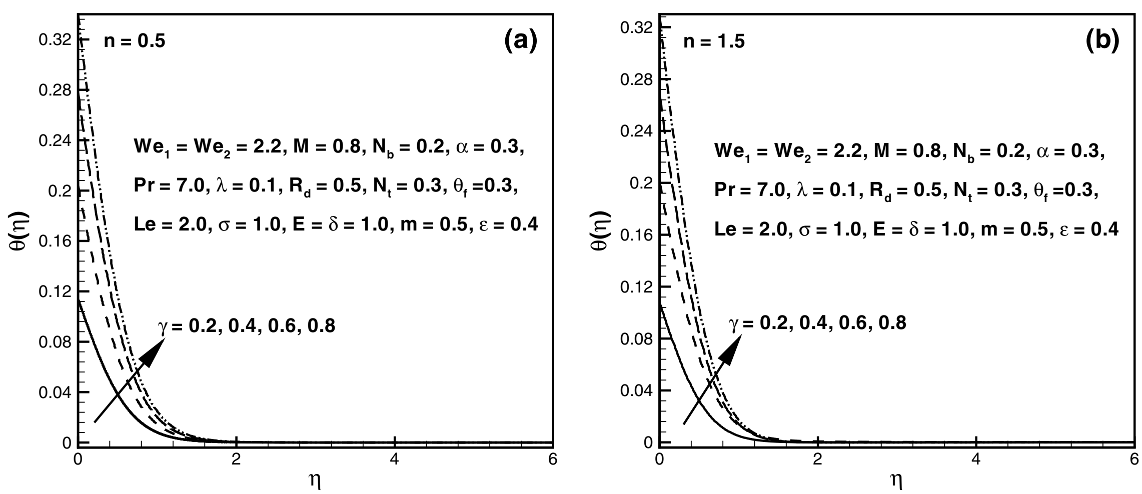

Fig. 8 Profiles of concentration $\theta(\eta)$ for various values of γ for shear-thinning (**a**) and shear-thickening liquids (**b**)

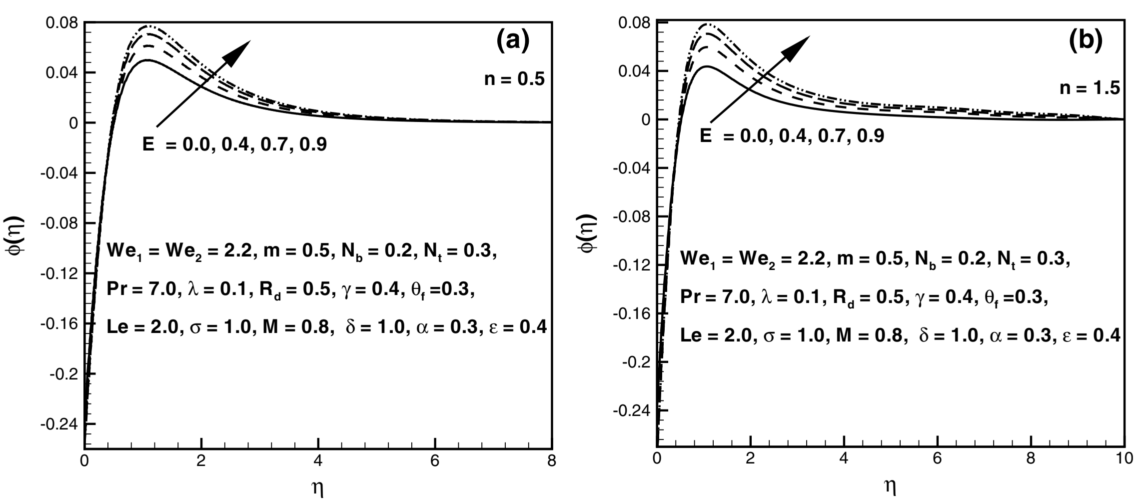

Fig. 9 Profiles of concentration $\varphi(\eta)$ for various values of E for shear-thinning (**a**) and shear-thickening liquids (**b**)

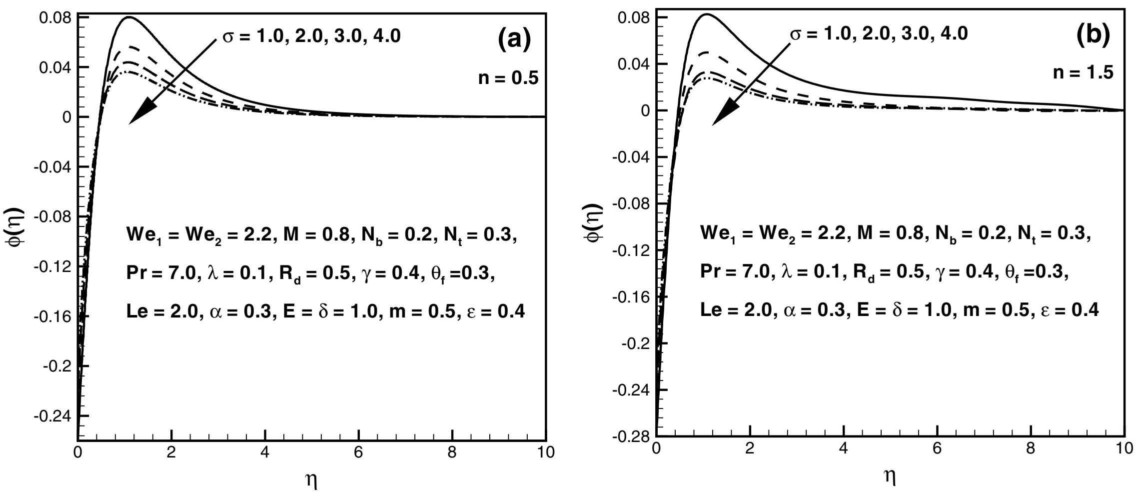

Fig. 10 Profiles of concentration $\varphi(\eta)$ for various values of σ for shear-thinning (**a**) and shear-thickening liquids (**b**)

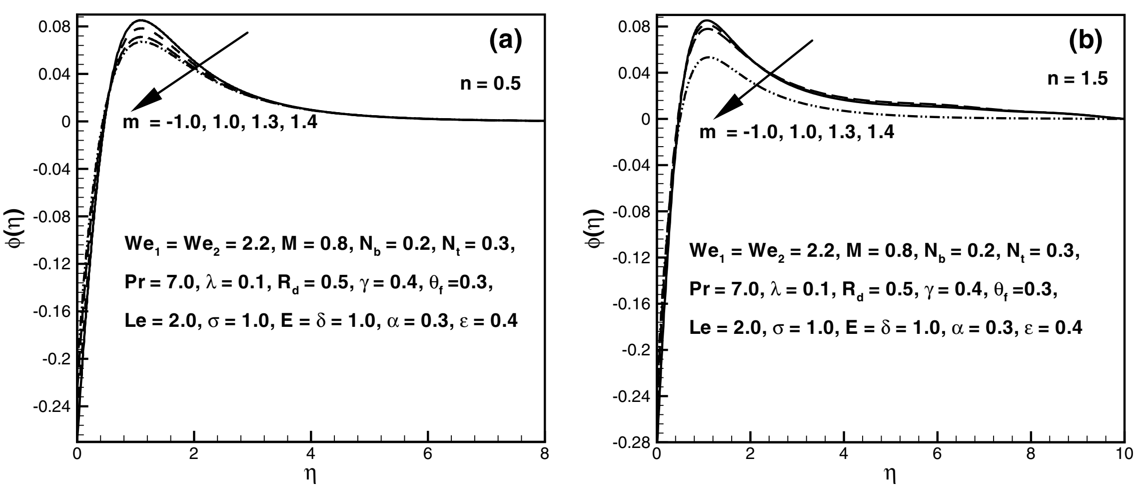

Fig. 11 Profiles of concentration $\varphi(\eta)$ for various values of m for shear-thinning (**a**) and shear-thickening liquids (**b**)

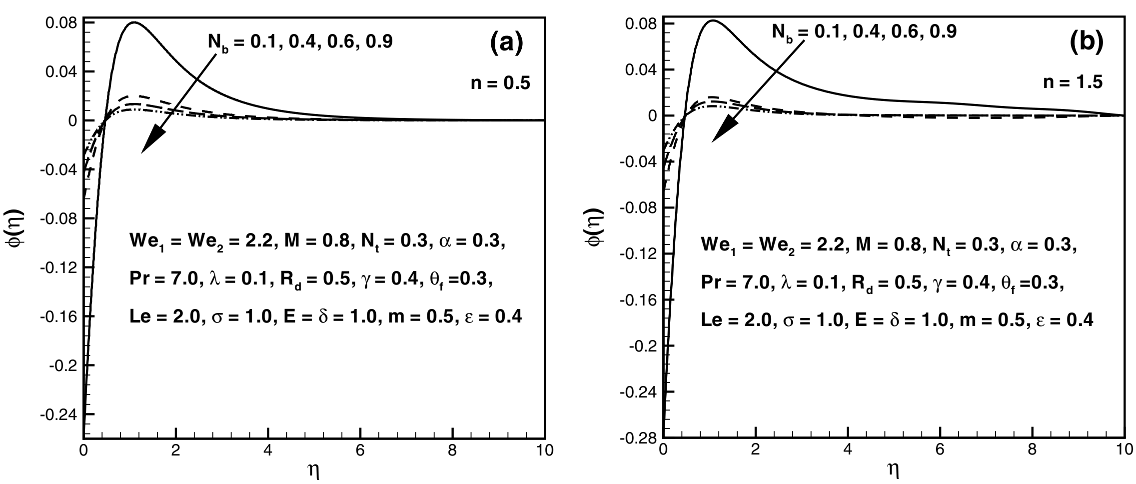

Fig. 12 Profiles of concentration $\varphi(\eta)$ for various values of N_{b} for shear-thinning (**a**) and shear-thickening liquids (**b**)

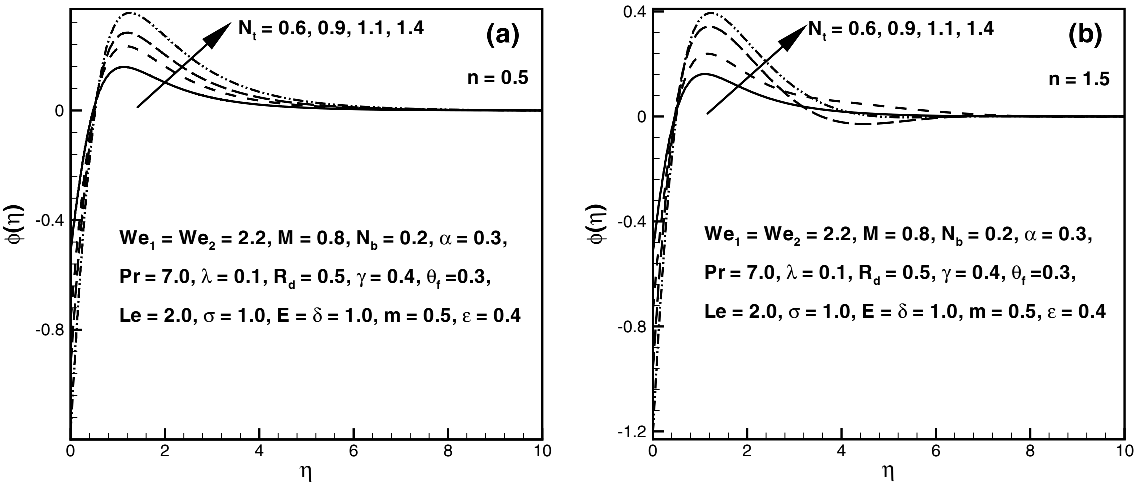

Fig. 13 Profiles of concentration $\varphi(\eta)$ for various values of N_t for shear-thinning (**a**) and shear-thickening liquids (**b**)

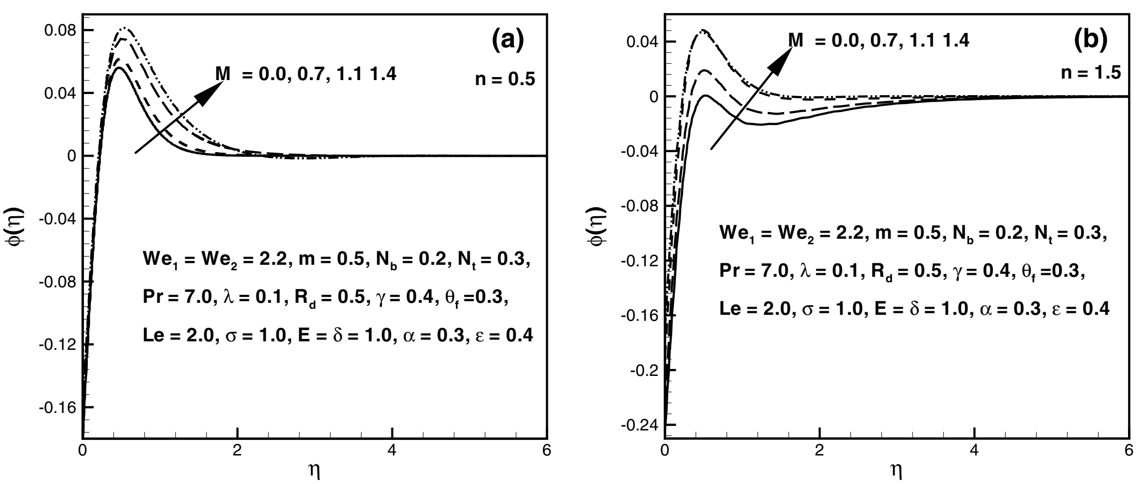

Fig. 14 Profiles of concentration $\varphi(\eta)$ for various values of M for shear-thinning (**a**) and shear-thickening liquids (**b**)

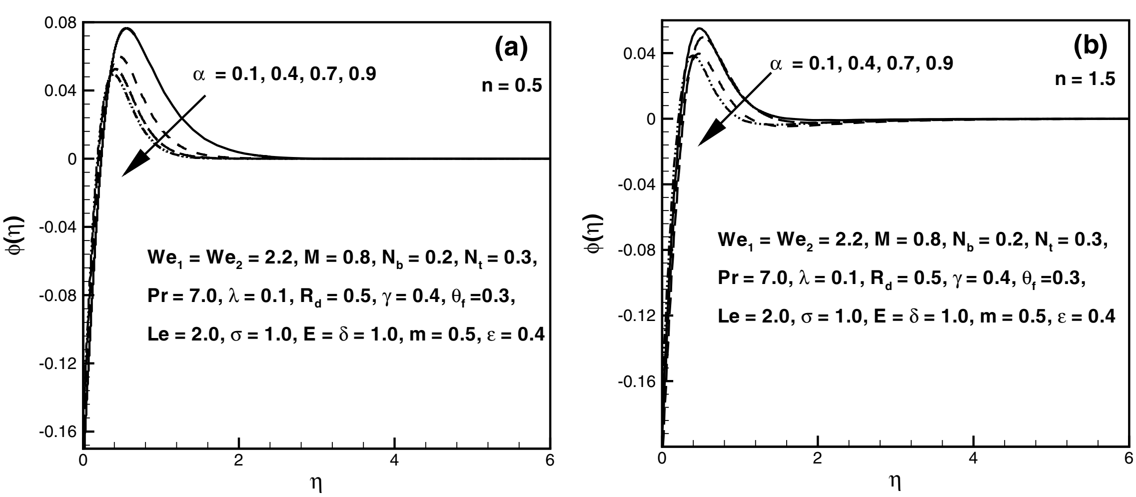

Fig. 15 Profiles of concentration $\varphi(\eta)$ for various values of α for shear-thinning (**a**) and shear-thickening liquids (**b**)

4.3 Concentration field

Figures 9, 10, 11, 12, 13, 14 and 15 are sketched to visualize the aspects of various physical parameters on concentration of cross-nanofluid. Concentration profiles of cross-nanofluid for different values of activation energy E are sketched through Fig. 9a, b. The growing values of E result in an augmentation in the concentration of cross-nanofluid. From the mathematical relation of Eq. (1), we detected that high activation energy and low temperature reduce the reaction rate due to which chemical reaction mechanisms slow down. Therefore, the concentration of cross-nanofluid enhances. The influence of chemical reaction parameter σ on the concentration profile is displayed in Fig. 10a, b. It is analyzed from these figures that the concentration profile declines with an increment in σ. Figure 11a, b is plotted to detect the characteristics of fitted rate constant m on concentration of cross-nanofluid. Chemically, as we boost up the values of m, destructive chemical mechanisms enhance due to concentration of cross-nanofluid declines. Figures 12a, b and 13a, b portray the concentration profile of cross-nanofluid for various vales of N_b and N_t. It is detected from these sketches that concentration of cross-nanofluid declines with elevation in N_t while the reverse trend is observed for N_b. Additionally, it is detected that physically, an uplift in the magnitude of N_b corresponds to rise in the rate at which nanoparticles in the base liquid move in random directions with different velocities. This movement of nanoparticles augments transfer of heat and therefore, declines the concentration profile. The influence of magnetic parameter M on the concentration profile of cross-fluid is displayed in Fig. 14a, b. It is analyzed from these figures that the concentration profile enhances with an increment in M. The concentration of cross-nanofluid increases due to heat produced by M. To investigate the aspects of the ratio of stretching rate parameter α on the concentration profile, we have plotted Fig. 15a, b. These figures reveal that the concentration profile declines as the value of α is augmented.

4.4 Quantities of physical interest

Tables 2 and 3 are presented to demonstrate the achieved outcomes for surface drag forces $\left(C_{f_x}, C_{f_y}\right)$ and heat transfer rates (Nu_x). It is noticed from Table 2 magnitude of surface drag forces is greater for larger estimation of n, α, M while opposite trend is observed for We_1 and We_2. Table 3 reveals that magnitude of heat transport rate deteriorates for augmented values of δ, σ, m and N_t, while it rises for Pr,E and n.

5 Main outcomes

Influence of Lorentz forces and chemical process on 3D flow of cross-nanofluid is investigated here. Impact of variable thermal conductivity on nanofluid is taken into consideration. Heat source–sink and thermal radiation mechanisms are deliberated here to characterize the heat transport mechanism. Influence of activation energy is considered. Main outcomes of this research work are pointed as

- Temperature of cross-nanofluid is an increasing function of N_t.
- Higher estimation of λ provides larger temperature of cross-nanofluid.
- An increment in α demonstrates decays in $\theta(\eta)$.

Table 2 Numerical values of local skin frictions $\left(-C_{fx}(Re_x)^{1/2}, -C_{fy}(Re_x)^{1/2}\right)$ for distinct values of escalating parameters

We_1	We_2	n	α	M	$-C_{fx}(Re_x)^{1/2}$	$-C_{fy}(Re_x)^{1/2}$
0.0	0.5	0.1	0.3	0.8	2.616613	0.6672313
0.2	–	–	–	–	1.394971	0.6644748
0.4	–	–	–	–	1.346258	0.6624166
0.5	0.6	–	–	–	1.330288	0.6611346
–	0.7	–	–	–	1.330100	0.6608477
–	0.8	–	–	–	1.329757	0.6607392
–	–	0.2	–	–	1.35598	0.7159371
–	–	0.3	–	–	1.394756	0.7773754
–	–	0.9	–	–	1.454798	0.8086462
–	–	–	0.4	–	1.347573	0.7259671
–	–	–	0.6	–	1.377045	0.9226853
–	–	–	0.8	–	1.404251	1.161177
–	–	–	–	1.0	1.458371	0.8344255
–	–	–	–	1.2	1.603129	1.00615
–	–	–	–	1.4	1.759637	1.187128

Table 3 Numerical values of Local Nusselt number $(Re_x)^{-\frac{1}{2}}Nu_x$ for distinct values of escalating parameters when $M = 0.8$, $We_1 = We_2 = 2.2$, $Le = 2.0$, $R_d = 0.5$, $\theta_f = 0.3$, $N_b = 0.2$, $\alpha = 0.3$ and $\gamma = 0.5$

Pr	E	δ	n	m	σ	N_t	$(Re_x)^{-1/2}Nu_x$
1.0	1.0	1.0	1.5	0.5	1.0	0.3	0.29044
2.0	–	–	–	–	–	–	0.324653
3.0	–	–	–	–	–	–	0.368596
–	0.0	–	–	–	–	–	0.35761
–	0.4	–	–	–	–	–	0.365915
–	0.7	–	–	–	–	–	0.367423
–	–	2.0	–	–	–	–	0.367447
–	–	3.0	–	–	–	–	0.36602
–	–	4.0	–	–	–	–	0.365904
–	–	–	0.2	–	–	–	0.33429
–	–	–	0.5	–	–	–	0.352049
–	–	–	0.8	–	–	–	0.346319
–	–	–	–	1.0	–	–	0.367526
–	–	–	–	1.3	–	–	0.367481
–	–	–	–	1.4	–	–	0.367465
–	–	–	–	–	1.0	–	0.367596
–	–	–	–	–	2.0	–	0.365712
–	–	–	–	–	3.0	–	0.362045
–	–	–	–	–	–	0.2	0.361876
–	–	–	–	–	–	0.4	0.36017
–	–	–	–	–	–	0.6	0.36000

- Concentration field enriches for intensifying estimation of M.
- Concentration of cross-magnetonanofluid augments for improving values of E.
- $\varphi(\eta)$ decays via m.
- The profiles of concentration descent for escalating m and σ.

References

1. Khan WA, Khan M, Malik R (2014) Three-dimensional flow of an Oldroyd-B nanofluid towards stretching surface with heat generation/absorption. PLoS ONE 9(8):e10510
2. Sheikholeslami M, Ellahi R (2015) Three dimensional mesoscopic simulation of magnetic field effect on natural convection of nanofluid. Int J Heat Mass Transf 89:799–808
3. Khan M, Khan WA (2015) Forced convection analysis for generalized Burgers nanofluid flow over a stretching sheet. AIP Adv 5:107138. https://doi.org/10.1063/1.4935043
4. Sandeep N, Kumar BR, Kumar MSJ (2015) A comparative study of convective heat and mass transfer in non-Newtonian nanofluid flow past a permeable stretching sheet. J Mol Liq 212:585–591
5. Rehman S, Haq RU, Khan ZH, Lee C (2016) Entropy generation analysis for non-Newtonian nanofluid with zero normal flux of nanoparticles at the stretching surface. J Taiwan Inst Chem Eng 63:226–235
6. Khan M, Khan WA (2016) MHD boundary layer flow of a power-law nanofluid with new mass flux condition. AIP Adv 6:025211. https://doi.org/10.1063/1.4942201
7. Haq RU, Khan ZH, Hussain ST, Hammouch Z (2016) Flow and heat transfer analysis of water and ethylene glycol based Cu nanoparticles between two parallel disks with suction/injection effects. J Mol Liq 221:298–304
8. Khan M, Khan WA (2016) Steady flow of Burgers' nanofluid over a stretching surface with heat generation/absorption. J Braz Soc Mech Sci Eng 38(8):2359–2367
9. Khan M, Khan WA, Alshomrani AS (2016) Non-linear radiative flow of three-dimensional Burgers nanofluid with new mass flux effect. Int J Heat Mass Transf 101:570–576
10. Rahman SU, Ellahi R, Nadeem S, Zaigham Zia QM (2016) Simultaneous effects of nanoparticles and slip on Jeffrey fluid through tapered artery with mild stenosis. J Mol Liq 218:484–493
11. Raju CSK, Sandeep N, Sugunamma V (2016) Unsteady magneto-nanofluid flow caused by a rotating cone with temperature dependent viscosity: a surgical implant application. J Mol Liq 222:1183–1191
12. Reddy JVR, Kumar KA, Sugunamma V, Sandeep N (2017) Effect of cross diffusion on MHD non-Newtonian fluids flow past a stretching sheet with non-uniform heat source/sink: a comparative study. Alex Eng J. https://doi.org/10.1016/j.aej.2017.03.008
13. Hayat T, Rashid M, Imtiaz M, Alsaedi A (2017) Nanofluid flow due to rotating disk with variable thickness and homogeneous–heterogeneous reactions. Int J Heat Mass Transf 113:96–105
14. Raju CSK, Hoque MM, Anika NN, Mamatha SU, Sharma P (2017) Natural convective heat transfer analysis of MHD unsteady Carreau nanofluid over a cone packed with alloy nanoparticles. Powder Technol 317:408–416

15. Khan M, Ahmad L, Khan WA (2017) Numerically framing the impact of radiation on magnetonanoparticles for 3D Sisko fluid flow. J Braz Soc Mech Sci Eng 39(11):4475–4487
16. Hayat T, Javed M, Imtiaz M, Alsaedi A (2017) Double stratification in the MHD flow of a nanofluid due to a rotating disk with variable thickness. Eur Phys J Plus 132:146
17. Khan M, Irfan M, Khan WA (2017) Impact of forced convective radiative heat and mass transfer mechanisms on 3D Carreau nanofluid: a numerical study. Eur Phys J Plus. https://doi.org/10.1140/epjp/i2017-11803-3
18. Kumar KA, Reddy JVR, Sugunamma V, Sandeep N (2017) Impact of frictional heating on MHD radiative ferrofluid past a convective shrinking surface. Defect Diffus Forum 378:157–174
19. Sandeep N (2017) Effect of aligned magnetic field on liquid thin film flow of magnetic-nanofluids embedded with graphene nanoparticles. Adv Powder Technol 28:865–875
20. Santhosh HB, Raju CSK (2018) Unsteady Carreau radiated flow in a deformation of graphene nanoparticles with heat generation and convective conditions. J Nanofluids 7:1130–1137
21. Anantha Kumar K, Ramana Reddy JV, Sugunamma V, Sandeep N (2018) Magnetohydrodynamic Cattaneo-Christov flow past a cone and a wedge with variable heat source/sink. Alex Eng J 57(1):435–444
22. Raju CSK, Saleem S, Mamatha SU, Hussain I (2018) Heat and mass transport phenomena of radiated slender body of three revolutions with saturated porous: Buongiorno's model. Int J Therm Sci 132:309–315
23. Khan WA, Alshomrani AS, Alzahrani AK, Khan M, Irfan M (2018) Impact of autocatalysis chemical reaction on nonlinear radiative heat transfer of unsteady three-dimensional Eyring–Powell magneto-nanofluid flow. Pramana J Phys. https://doi.org/10.1007/s12043-018-1634-x
24. Anantha Kumar K, Sugunamma V, Sandeep N, Ramana Reddy JV (2018) Impact of Brownian motion and thermophoresis on bio convective flow of nanoliquids past a variable thickness surface with slip effects. Multidiscip Model Mater Struct. https://doi.org/10.1108/MMMS-02-2018-0023
25. Kumar KA, Reddy JVR, Sugunamma V, Sandeep N (2018) Impact of cross diffusion on MHD viscoelastic fluid flow past a melting surface with exponential heat source. Multi Mod Mat Str. https://doi.org/10.1108/MMMS-12-2017-0151
26. Santhosh HB, Raju CSK (2018) Carreau fluid over a radiated shrinking sheet in a suspension of dust and titanium alloy nanoparticles with heat source. J Integr Neurosci. https://doi.org/10.3233/jin-180083
27. Santhosh HB, Raju CSK (2018) Partial slip flow of radiated Carreau dusty nanofluid over exponentially stretching sheet with non-uniform heat source or sink. J Nanofluids 7:72–81
28. Alshomrani AS, Ullah MZ, Capizzano SS, Khan WA, Khan M (2018) Interpretation of chemical reactions and activation energy for unsteady 3D flow of Eyring–Powell magneto-nanofluid. Arab J Sci Eng. https://doi.org/10.1007/s1336
29. Anantha Kumar K, Ramana Reddy JV, Sugunamma V, Sandeep N (2018) Simultaneous solutions for MHD flow of Williamson fluid over a curved sheet with non-uniform heat source/sink. Heat Transf Res. https://doi.org/10.1615/heattransres.2018025939
30. Durgaprasad P, Varma SVK, Hoque MM, Raju CSK (2018) Combined effects of Brownian motion and thermophoresis parameters on three-dimensional (3D) Casson nanofluid flow across the porous layers slendering sheet in a suspension of graphene nanoparticles. Neural Comput Appl. https://doi.org/10.1007/s00521-018-3451-z
31. Ramadevi B, Sugunamma V, Kumar KA, Reddy JVR (2018) MHD flow of Carreau fluid over a variable thickness melting surface subject to Cattaneo-Christov heat flux. Multi Mod Mat Str. https://doi.org/10.1108/MMMS-12-2017-0169
32. Saleem S, Nadeem S, Rashidi MM, Raju CSK (2018) An optimal analysis of radiated nanomaterial flow with viscous dissipation and heat source. Microsyst Technol. https://doi.org/10.1007/s00542-018-3996-x
33. Anantha Kumar K, Reddy JVR, Sugunamma V, Sandeep N (2018) MHD flow of chemically reacting Williamson fluid over a curved/flat surface with variable heat source/sink. Int J Fluid Mech Res. https://doi.org/10.1615/interjfluidmechres.2018025940
34. Upadhya SM, Raju CSK, Saleem S, Alderremy AA (2018) Modified Fourier heat flux on MHD flow over stretched cylinder filled with dust, graphene and silver nanoparticles. Results Phys 9:1377–1385
35. Anantha Kumar K, Ramadevi B, Sugunamma V (2018) Impact of Lorentz force on unsteady bio convective flow of Carreau fluid across a variable thickness sheet with non-Fourier heat flux model. Defect Diffus Forum 387:474–497
36. Irfan M, Khan M, Khan WA, Ayaz M (2018) Modern development on the features of magnetic field and heat sink/source in Maxwell nanofluid subject to convective heat transport. Phys Lett A 382(30):1992–2002
37. Lakshmi KB, Kumar KA, Reddy JVR, Sugunamma V (2019) Influence of nonlinear radiation and cross diffusion on MHD flow of Casson and Walters-B nanofluids past a variable thickness sheet. J Nanofluids 8:73–83
38. Khan WA, Khan M, Alshomrani AS (2016) Impact of chemical processes on 3D Burgers fluid utilizing Cattaneo-Christov double-diffusion: applications of non-Fourier's heat and non-Fick's mass flux models. J Mol Liq 223:1039–1047
39. Khan WA, Alshomrani AS, Khan M (2016) Assessment on characteristics of heterogeneous–homogeneous processes in three-dimensional flow of Burgers fluid. Results Phys 6:772–779
40. Khan MI, Waqas M, Hayat T, Imran Khan M, Alsaedi A (2017) Numerical simulation of nonlinear thermal radiation and homogeneous–heterogeneous reactions in convective flow by a variable thicked surface. J Mol Liq 246:259–267
41. Khan MI, Waqas M, Hayat T, Imran Khan M, Alsaedi A (2017) Chemically reactive flow of upper-convected Maxwell fluid with Cattaneo-Christov heat flux model. J Braz Soc Mech Sci Eng 39(11):4571–4578
42. Khan WA, Irfan M, Khan M, Alshomrani AS, Alzahrani AK, Alghamdi MS (2017) Impact of chemical processes on magneto nanoparticle for the generalized Burgers fluid. J Mol Liq 234:201–208
43. Mustafa M, Khan JA, Hayat T, Alsaedi A (2017) Buoyancy effects on the MHD nanofluid flow past a vertical surface with chemical reaction and activation energy. Int J Heat Mass Transf 108:1340–1346
44. Ariel PD (2007) The three-dimensional flow past a stretching sheet and the homotopy perturbation method. Comput Math Appl 54:920–925